Postnatal neuronal *Bace1* deletion impairs neuroblast and oligodendrocyte maturation

Marc R. Benoit, Mabintou Darboe, Brati Das, Yingying Ge, John Zhou, Annie Yao, Wanxia He, Riqiang Yan 🄳 and Xiangyou Hu*

Department of Neuroscience, University of Connecticut Health Center, Farmington, CT 06030, USA

*To whom correspondence should be addressed at: Department of Neuroscience, University of Connecticut Health Center, 263 Farmington Ave, Farmington, CT 060303401, USA. Tel: +1-860-679-3527; Fax: +1-860-679-8766; Email: xhu@uchc.edu and riyan@uchc.edu

Abstract

Beta amyloid cleaving enzyme 1 (BACE1) is largely expressed by neurons and is the sole β-secretase for initiating the production of neuronal β-amyloid peptides (Aβ). To fully understand the physiological functions of neuronal BACE1, we used mouse genetic approach coupled with unbiased single nucleus RNA sequencing (snRNAseq) to investigate how targeted deletion of *Bace1* in neurons, driven by Thy-1-Cre recombinase, would affect functions in the nervous system. Our transcriptome results revealed that BACE1 is essential for maturation of neural precursor cells and oligodendrocytes in mice. RNA velocity analysis confirmed deficit in the trajectory of neuroblasts in reaching the immature granule neuron state in young *Bace1*$^{fl/fl}$; *Thy1*-cre mice. Further analysis of differential gene expression indicated changes in genes important for SNARE signaling, tight junction signaling, synaptogenesis and insulin secretion pathways. Morphological studies revealed a hypomyelination in *Bace1*$^{fl/fl}$;*Thy1*-cre sciatic nerves, but no detectable myelination changes in the corpus callosum, despite clear reduction in myelination proteins in the brain. Functional studies showed reduction in long-term potential, defects in synaptogenesis and learning behavioral. Altogether, our results show that neuronal BACE1 is critical for optimal development of central and peripheral nervous system, and inhibition of neuronal BACE1 will result in deficits in synaptic functions and cognitive behaviors.

Graphical Abstract
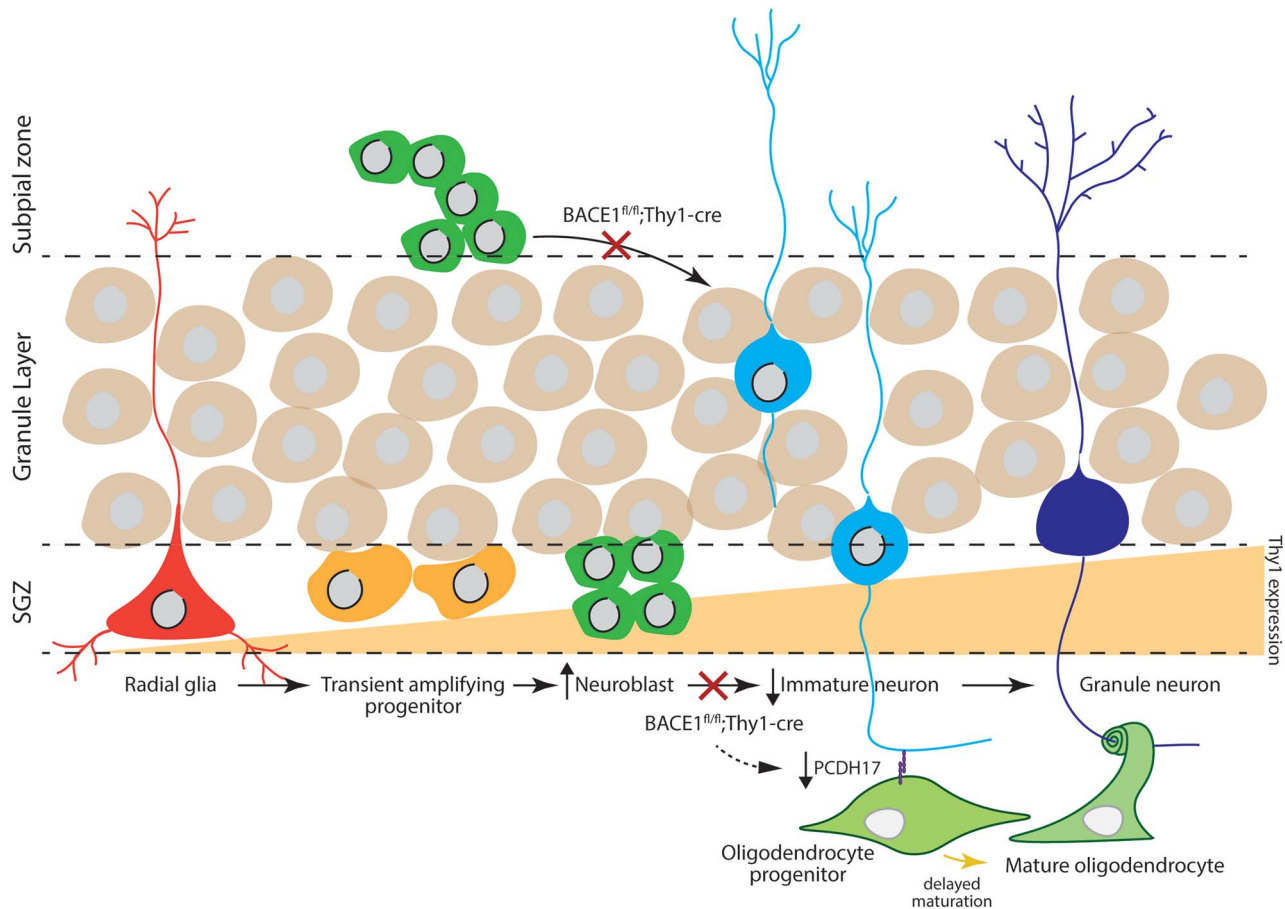
Neurogenic niches in the hippocampus showing Thy1-dependent knockout of *Bace1* resulting in inhibition of neuroblast migration and maturation from the subpial zone and subgranular zone. This results in a relative increase in neuroblasts in *Bace1*^{fl/fl};*Thy1*-cre mice. BACE1 loss from neurons leads to a decrease in neuronal PCDH17, potentially affecting communication between neurons and myelinating oligodendrocytes leading to delayed maturation of both neurons and oligodendrocytes.

Introduction

Alzheimer's disease (AD) is a debilitating and prevalent form of dementia, largely due to abnormal accumulation of amyloid-β peptide (Aβ) in senile plaques and aggregated tau proteins in neurofibrillary tangles. It is well established that production of Aβ and accumulation of Aβ-containing plaques drives the pathogenesis of AD (1,2); thus, Aβ production and clearance has been one of the focuses for AD treatment (3,4).

Aβ is produced from the proteolytic processing of the type-1 transmembrane protein: amyloid precursor protein (APP) (5). Upon insertion into the membrane, APP is sequentially cleaved by β- and γ-secretase, releasing the Aβ40 and Aβ42 fragments into the extracellular space with Aβ42 being more neurotoxic (6). β-Site APP cleaving enzyme 1 (BACE1) is the rate-limiting β-secretase, predominantly responsible for producing Aβ (7–9), and thus is a therapeutic target for disease-modifying drugs. While *Bace1* deletion results in drastic reduction of plaque formation (10–12), APP is just one of many proteolytic targets of BACE1. The safety of BACE1 inhibition has become a concern due to abolished cleavage of its substrates responsible for normal neuronal functions (13–15). *Bace1*-null mice exhibit smaller postnatal size and reduced muscle coordination (16,17), memory deficits (18,19), hypomyelination (20–22), abnormal EEG activity and spontaneous seizures (23,24), axon guidance defects (25–28) and other

debilitating phenotypes due to the role of BACE1 in rodent development (29). In addition, BACE1 is not only a neuronal protein but is widely expressed in oligodendrocytes, astrocytes and microglia, and its role in microglia appears to regulate the transition from homeostatic signature to stage-1 disease associated microglia (30). Considering BACE1 has cell type-specific and cell autonomous roles in both embryonic development and adulthood, we aimed to investigate the consequences of *Bace1* conditional knockout specific to postnatal neurons.

To this end, we generated neuron-specific deletion of *Bace1* in the central nervous system by crossing *Bace1*^{fl/fl} mice with *Thy1-cre* mice (JAX #006143) (31), and examined transcriptomic profiles using single-nuclear RNA sequencing (snRNA-Seq). Our transcriptome results revealed altered adult neurogenic stem cell pools and oligodendrocyte maturation. We further followed up with biochemical and imaging assays to confirm these changes on neuronal activity and behaviors. We observed an increased number of neuronal precursors in the hippocampus, differentially expressed genes involved in synaptogenesis and synaptic adhesion, hypomyelination of sciatic nerve axons, behavioral deficits and deficits in long-term potentiation (LTP). This constellation of phenotypes resulting from postnatal deletion of Bace1 in neurons suggests a non-cell autonomous effect on cell maturation and a cell-autonomous effect on neuronal activity. These findings

demonstrate concordance of single-cell and single-nuclear RNA sequencing data in its use for revealing cell fate trajectory. More broadly, these data allow us to further understand the role of neuronal BACE1 in neurogenesis and gliogenesis.

Results

Single-nuclear RNA sequencing of *Bace1*^fl/fl^;*Thy1*-Cre hippocampi reveals shifts in maturation of neural progenitor cells and oligodendrocytes

To investigate the effect of *Bace1* deletion in neuronal populations, we generated a *Bace1*^fl/fl^;*Thy1*-cre mouse. Protein levels of BACE1 were visibly reduced in hippocampal lysates prepared from postnatal day 28 (P28) and P114 *Bace1*^fl/fl^;*Thy1*-cre mice (Fig. 1A). Levels of full-length APP were elevated (Fig. 1A and B), consistent with the corresponding reduction in C-terminal fragment (C-99), released after BACE1-cleavage of APP. Quantification confirmed these changes in protein levels (Fig. 1B).

To understand how neuronal deletion of *Bace1* would impact hippocampal function, we performed snRNA-Seq on eight hippocampi from four male and four female mice (age P31 and P192) to compare transcriptomic profiles from *Bace1*^fl/fl^ and *Bace1*^fl/fl^;*Thy1*-cre littermates (Fig. 1C). We chose to perform snRNA-Seq over single-cell RNA sequencing (scRNA-Seq) because of the reduced bias in cellular coverage and the improved isolation of neuronal subtypes (32,33). Sequencing resulted in a total of 62,734 nuclei (average 7,842 per mouse) with an average of 2,000 RNA counts per nucleus. Based on expression of canonical cell type markers, we were able to identify UMAP-clustered nuclei as representing typical cells found in the adult mouse hippocampus (Fig. 1C and D). *Bace1* deletion in neurons did not obviously change the population of nuclei: identified as 60% neurons, 17% oligodendrocytes, 8% astrocytes, 5% microglia and the remainder as progenitors and endothelial cells. When comparing cell type abundance between the two control age groups, *Bace1*^fl/fl^ P31 and *Bace1*^fl/fl^ P192, as expected, we noted a decrease in the proportion of radial glia (3.1% at P31 to 1.3% at P192), neuroblasts (5.3% at P31 to 0.4% at P192) and committed oligodendrocyte precursors (COPs) (1.3% at P31 to 0.4% at P192), and a concomitant increase in proportion of mature oligodendrocytes in the older age group (3.8% at P31 to 17.3% at P192) (Fig. 1E). This suggested to us the abundance of cell types captured with snRNAseq reflects the change in cell types as mice age from P31 to P192. Newly formed oligodendrocytes (NFOLs) were not obviously changed between P31 and P192 mice, but NFOLs in *Bace1*^fl/fl^;*Thy1*-cre mice were generally less when compared with *Bace1*^fl/fl^ littermates.

When comparing cell type abundances between *Bace1*^fl/fl^ and *Bace1*^fl/fl^;*Thy1*-cre mice, we noted the largest effect at the P31 age. We observed a 1.2-fold increase in the number of neuroblasts (defined as DCX^+^ nuclei) when *Bace1* was deleted from neurons (5.3% ± 0.27 of total nuclei for Bace1^fl/fl^ compared with 6.3% ± 0.25 for *Bace1*^fl/fl^;*Thy1*-cre, Fig. 1E). Interestingly, *Thy1* expression was not detectable until neuroblasts matured into immature granule neurons (Fig. 1D). This observation is consistent with the data presented by Alić *et al.*, who found in a Thy1-YFP mouse that YFP was only detected after nestin-positive neural stem cells began to differentiate into immature neurons (34). Our data suggest that the deletion of *Bace1* is either preventing the maturation of neuroblasts in a cell autonomous manner or increasing the proliferation of radial glia down the neural lineage in a non-cell autonomous manner. We also noted a 1.2-fold decrease in COPs

compared to controls (1.3% ± 0.05 for P31 *Bace1*^fl/fl^ to 1.1% ± 0.2 for P31 *Bace1*^fl/fl^;*Thy1*-cre) and a 1.3-fold decrease in NFOLs (7.4% ± 0.2 for P31 *Bace1*^fl/fl^ to 5.8% ± 0.3 for P31 *Bace1*^fl/fl^;*Thy1*-cre) (Fig. 1E). The abundance of mature oligodendrocytes was also reduced by 2.1-fold with neuronal BACE1 deletion at the P31 time point (3.8% ± 0.04 for *Bace1*^fl/fl^ to 1.8% ± 0.6 for P31 *Bace1*^fl/fl^;*Thy1*-cre) (Fig. 1E). Our observation of decreased COPs, NFOLs and mature oligodendrocytes at P31 suggests a delay of oligodendrocyte maturation in a non-cell autonomous manner when *Bace1* is deleted by Cre driven by a Thy-1 promoter.

RNA velocity reveals BACE1 substrates responsible for the maturation of neuroblasts

In the adult hippocampus, radial glia-like cells have the ability to differentiate into glia and neuroblasts, which migrate into the granule cell layer and mature into fully functional excitatory granule cells (35,36). This process has been well-characterized using single-cell transcriptomics (37). Since we observed an accumulation of neuroblasts in the hippocampus in response to neuronal *Bace1* deletion, we explored the state of cells as they transitioned from radial glia to granule neurons to further understand which genes are likely critical to this process and if BACE1 plays a role. To this end, we employed single-cell velocity: a measurement of pre-mature (unspliced) and mature (spliced) mRNA transcripts, a method used to determine cell trajectory (38). Astrocytes (AQP4^+^), radial glia (PTPRZ^+^), neuroblasts (DCX^+^), immature and mature granule neurons (PROX1^+^/SLC17a7^+^) were plotted from our initial clustering analysis and measured using pseudotime, a velocity-inferred transition matrix that computes distances from a root cell (Fig. 2A, top). In the P31 control samples, we observed an obvious transition of cells with a root in radial glia and end points at astrocytes and granule neurons, matching previously reported RNA velocity analysis of mouse hippocampus (39). To our knowledge, this is the first report of single-nuclear RNA sequencing data showing concordance with single-cell RNA sequencing of the hippocampus, suggesting the measurement of spliced:unspliced transcripts to determine RNA velocity can be accomplished using nuclear RNA. This was further demonstrated using an unbiased partition-based graph abstraction (PAGA), which correctly inferred cell trajectories rooted in radial glia (Fig. 2B, top). When measuring pseudotime of the P31 *Bace1*^fl/fl^;*Thy1*-cre mice, we observed an obvious deficit in the trajectory of neuroblasts, suggesting a decreased differentiation of the neuroblasts into granule neurons (Fig. 2A, bottom). Using PAGA, we also observed a failure in neuroblasts reaching the immature granule neuron state (Fig. 2B, bottom).

To confirm the observation of neuroblasts impaired to differentiate, we conducted immunohistochemical staining of P28 *Bace1*^fl/fl^ and *Bace1*^fl/fl^;*Thy1*-cre hippocampal sections with Dcx, NeuN and SMI22. A striking increase in the number of DCX^+^ cells in the subgranular zone of *Bace1*^fl/fl^;*Thy1*-cre mice was noted (Fig. 2C), as well as DCX^+^ cells outside of the subgranular zone (Fig. 2C, specified with an arrow), suggesting a failure of migration of neural progenitors as previously observed with global Bace1^−/−^ from the subpial zone (40). We also noted increased ramification of radial glia within the granule layer of the dentate gyrus, consistent with the abundances of cell types observed from our snRNAseq results.

To determine which genes displayed differential velocity between *Bace1*^fl/fl^ and *Bace1*^fl/fl^;*Thy1*-cre mice, we performed a differential velocity expression test using the Welch t-test (39). We found most genes with differential velocity played a role in neuronal development and were transcriptionally regulated
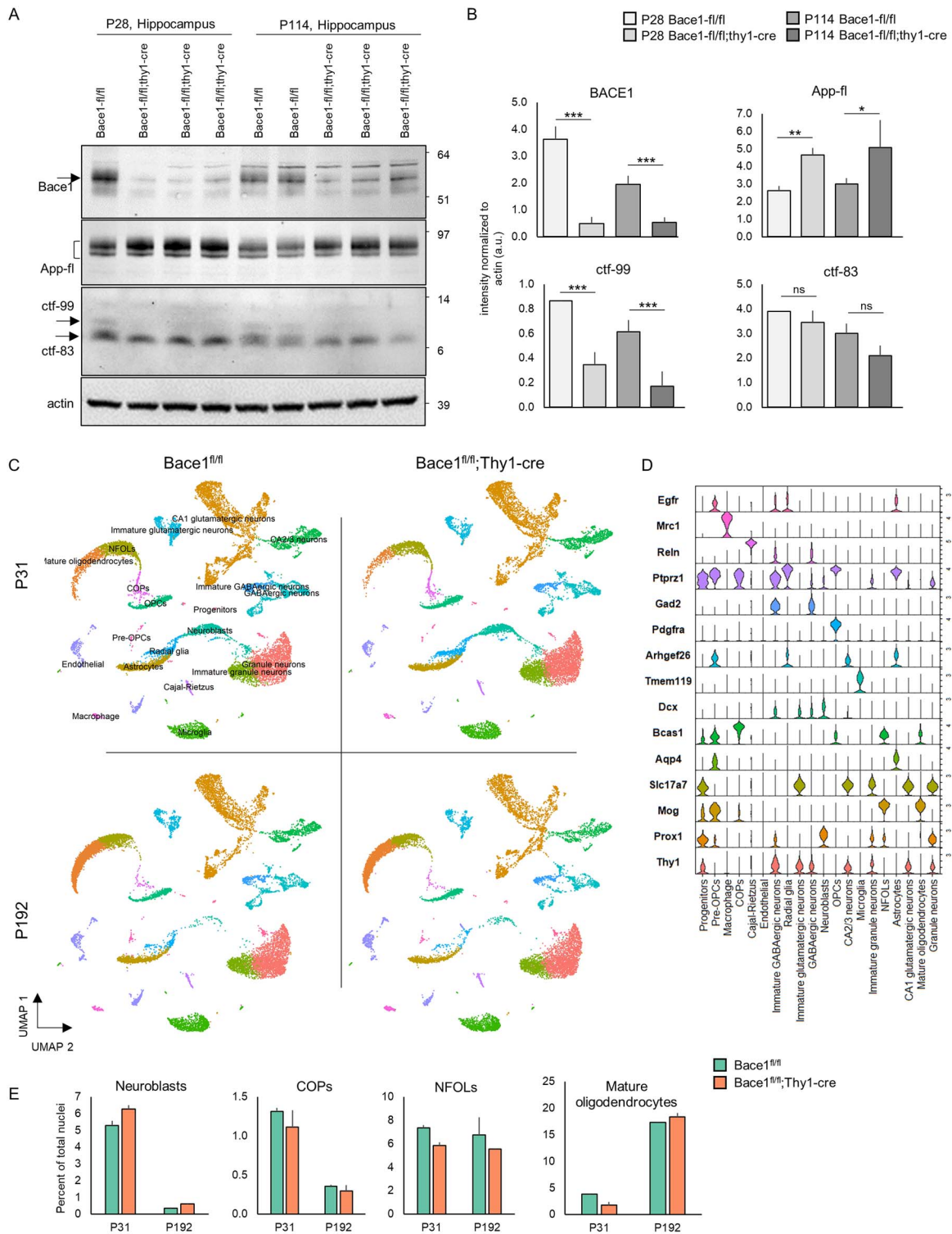
Figure 1. (**A**) Western blot of BACE1, App-full length and its c-terminal fragments, ctf-99 and ctf-83, from P28 and P114 *Bace1*^fl/fl and *Bace1*^fl/fl;*Thy1*-cre hippocampal lysates. (**B**) Quantification of BACE1, App and its c-terminal fragment protein levels after neuronal deletion of *Bace1* from western blots. (**C**) UMAP clusters of single nuclear sequencing from eight mouse hippocampii: one male and one female P31 *Bace1*^fl/fl, one male and one female P31 *Bace1*^fl/fl;*Thy1*-cre, one male and one female P192 *Bace1*^fl/fl, and one male and one female P192 *Bace1*^fl/fl;*Thy1*-cre. (**D**) Canonical cell type markers denoting cluster cell type identities in 1C. (**E**) Quantification of the number of sequenced nuclei as percent of total per animal, revealing a shift in the fraction of nuclei by cell type between P31 and P192 mice.

within immature granule neurons (Fig. 2D). Of this list, two genes with differential velocity are known to be BACE1 substrates: SEZ6L and OPCML (13,41,42). SEZ6L and OPCML possessed high velocity specific to immature granule neurons, and showed

a velocity reduction in *Bace1*^fl/fl;*Thy1*-cre (P-value = 0.020 and 0.019, respectively (Fig. 2D, arrows and E). Functional studies have revealed that the SEZ6 family is required for normal dendritic arborization of cortical neurons and synaptic function,
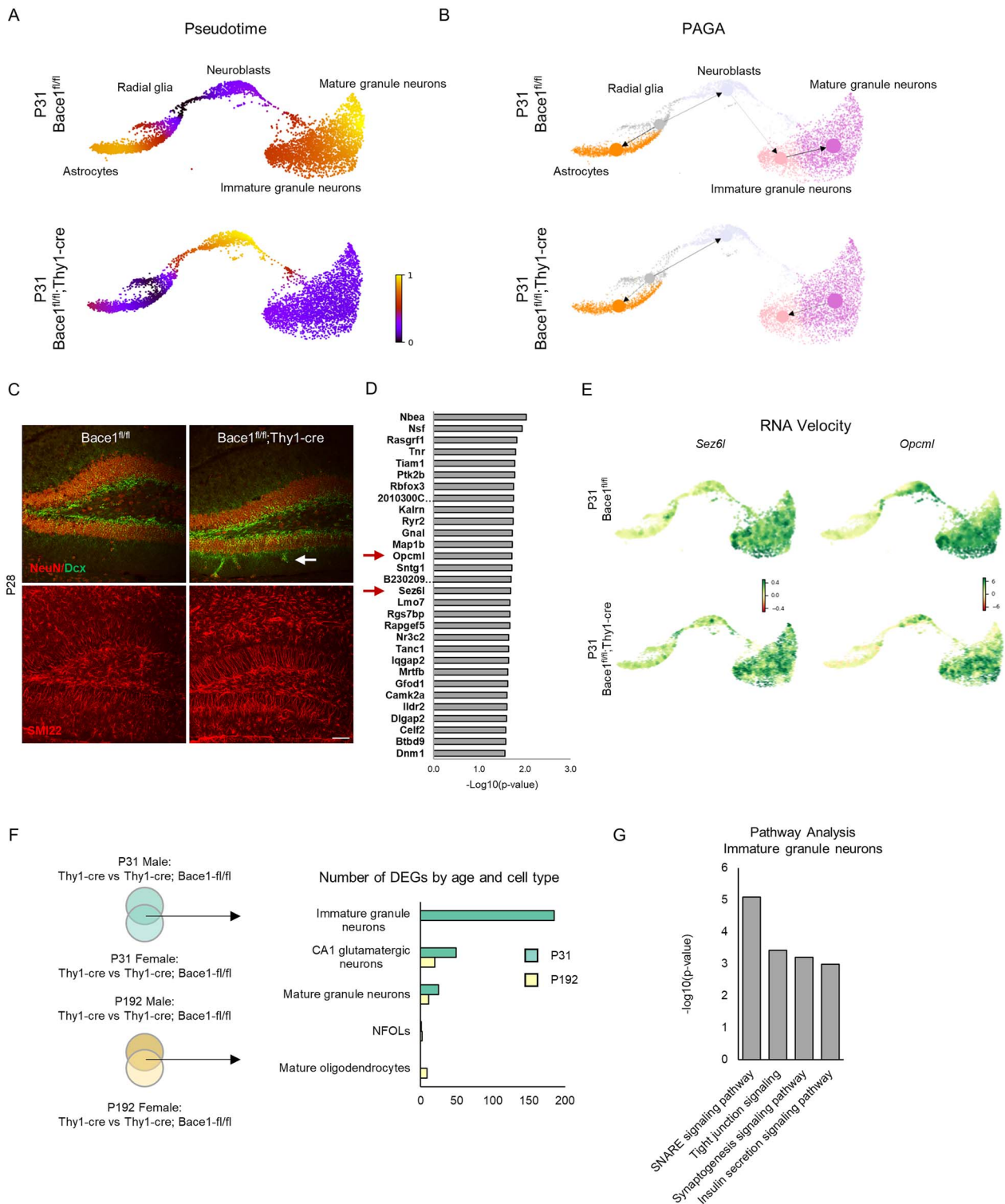
Figure 2. (**A**) Isolated UMAP plots of astrocytes, radial glia, neuroblasts, immature granule neurons and mature granule neurons from P31 *Bace1*^{fl/fl} (top) and P31 *Bace1*^{fl/fl};*Thy1*-cre (bottom). Colors denote cell trajectory in pseudotime, representing distance from a root cell. (**B**) Partition-based graph abstraction (PAGA) of UMAP plots from A revealing the trajectory of cell types originating from radial glia and developing toward the astrocyte lineage or granule neuron lineage. (**C**) Immunohistochemistry of P28 *Bace1*^{fl/fl} and *Bace1*^{fl/fl};*Thy1*-cre hippocampal sections stained with NeuN, Dcx or SMI22. Scale bar = 50 μm. (**D**) Differential velocity test between P31 *Bace1*^{fl/fl} and P31 *Bace1*^{fl/fl};*Thy1*-cre nuclei within immature granule neurons reveals significantly altered genes in their RNA velocity. Two are known BACE1 substrates (arrows). (**E**) Representative RNA velocity plots of Sez6l and Opcml between P31 *Bace1*^{fl/fl} and P31 *Bace1*^{fl/fl};*Thy1*-cre. (F, left) Strategy for performing differential gene expression testing between eight mice. (**F**, right) The number of significant differentially expressed genes by age and by cell type between *Bace1*^{fl/fl} and *Bace1*^{fl/fl};*Thy1*-cre mice. (**G**) Ingenuity Pathway Analysis (IPA) of the differentially expressed genes within P31 immature granule neurons.

and OPCML is required for neurite outgrowth and cell surface recognition during brain development (43–46). These data suggest that neuronal *Bace1* deletion results in a failure of neuroblasts to mature into immature granule neurons due to a deficit in immature granule neuron maturation.

Since neuronal *Bace1* deletion altered neuronal migration and maturation, we wondered if the transcriptome was altered and within which cell types. We then performed differential expression analysis using MAST (Model-based Analysis of Single-cell Transcriptomics) (33,47) between control and *Bace1*^fl/fl^;*Thy1*-cre samples. To increase the specificity of our differential gene analysis, we utilized our two *Bace1*^fl/fl^ animals and two *Bace1*^fl/fl^;*Thy1*-cre animals per age group to independently analyze each pair. Only genes that were altered consistently between both comparisons with a Bonferroni-corrected *P*-value were retained (Fig. 2F, left). Immature granule neurons from P31 mice possessed the majority of differentially expressed genes between *Bace1*^fl/fl^ and *Bace1*^fl/fl^;*Thy1*-cre (107 increased, 78 decreased), while the P192 age group had very few differentially expressed genes, suggesting that Bace1-KO had more of an effect on younger animals (Fig. 2F, right). Pathway analysis by utilizing ingenuity pathway analysis (IPA, Qiagen) revealed significant changes to SNARE signaling, tight junction signaling, synaptogenesis and insulin secretion pathways (Fig. 2G).

Taken together, we have found, through unbiased snRNA-Seq and RNA velocity approaches, that neuronal *Bace1* deletion results in an accumulation of neuroblasts that fail to timely differentiate into immature granule neurons. In addition, several BACE1 substrates are transcriptionally active while transitioning cells from radial glia to granule neurons. Since these BACE1 targets are critical for synaptic development, neuron migration and neuron maturation, we postulate that the increase in neuroblasts and their failed migration in *Bace1*^fl/fl^;*Thy1*-cre hippocampus is due to lack of processing of these BACE1 substrates. Since the recombination of floxed-*Bace1* is regulated by *Thy1* expression, we are observing an effect of *Bace1* deletion after neuroblasts begin to transition into immature granule neurons. This is further exemplified by the observation that the most significant change to the transcriptome in *Bace1*^fl/fl^;*Thy1*-cre animals occurs within immature granule neurons. Differential gene expression and differential RNA velocity due to neuronal *Bace1* deletion is the highest within immature granule neurons and reveals a perturbation to SNARE signaling, tight junction signaling, synaptogenesis and insulin signaling pathways, all which point to a deficit in migration, maturation and synaptic dysfunction.

Altered synaptic gene expression in *Bace1*^fl/fl^;*Thy1*-Cre hippocampi

To further investigate the effect of *Bace1* deletion on synaptic function, we investigated which synaptic genes within immature granule neurons were differentially expressed compared to controls. While the majority of differentially expressed genes had a modest log2 fold change of ±0.2, we observed a large decrease in protocadherin 17 (Pcdh17) expression in *Bace1*^fl/fl^;*Thy1*-cre animals specific to granule neurons, despite its high expression in COPs (Fig. 3A–C). This finding is intriguing because protocadherin 17 (PCDH17) mediates presynaptic assembly and axon extension, and has recently been predicted to be a BACE1 substrate (42,48,49). Consistent with the reduction of *Pcdh17* mRNA, its protein levels in hippocampal lysates of P28 *Bace1*^fl/fl^;*Thy1*-cre animals were lower than that of *Bace1*^fl/fl^ controls (Fig. 3D). Using two different PCDH17 antibodies, we noted a reduction in the full-length

isoform and its predicted cleaved fragment (60 kDa), consistent with the notion that PCDH17 is a BACE1 substrate in neurons (quantification validated in Fig. 3D).

Considering the role of PCDH17 in presynaptic assembly and our previous report of BACE1 in the control of synaptic vesicle release (50), we performed electron microscopy to examine the synapses of *Bace1*^fl/fl^;*Thy1*-cre mouse Schaffer collateral:CA1 pathway, including measurement of active zone length, docked vesicles and total number of vesicles in the readily releasable pool. We found a significant decrease in all parameters when *Bace1* was knocked out in neurons (Fig. 3E and F). In comparing to global *Bace1*-null mouse synapses, the number of docked vesicles and total number of vesicles in the readily releasable pool were similarly reduced, but the active zone length was surprisingly increased, rather than reduced in the Bace1-null synapses, suggesting a possible contribution of non-neuronal BACE1 in the formation of active zone length (Fig. 3F). In line with this morphological alteration, LTP at the Schaffer collateral:CA1 region of *Bace1*^fl/fl^;*Thy1*-cre mice significantly reduced compared with *Bace1*^fl/fl^ controls (Fig. 3G). Our findings suggest a cell-autonomous role of BACE1 in pre-synaptic vesicle dynamics and dysregulation of genes involved in synaptogenesis.

Bace1^fl/fl^;*Thy1*-Cre mice exhibit myelination deficits

Bace1-null mice have been shown to have weak deficits in optic nerve myelination, but this defect was not obvious in the zebrafish model (21,51). In our unbiased snRNAseq data analysis, we noted a reduction in the abundance of COPs, NFOLs and mature oligodendrocytes in P31 *Bace1*^fl/fl^;*Thy1*-cre mice (Fig. 1E), suggesting a neuronally derived signal for inhibiting oligodendrocyte maturation. To determine if neuronal *Bace1* deletion changed the transcriptome of these cell types, we noted only several upregulated genes in P192 *Bace1*^fl/fl^;*Thy1*-cre mature oligodendrocytes (Fig. 4A), including prostaglandin D2 synthase (*Ptgds*) and apolipoprotein E (*ApoE*) (Fig. 4B). Interestingly, Ptgds is upregulated in response to neuregulin 1-ICD, a Bace1 cleavage product, and plays a role in myelination (52). ApoE has also been shown to facilitate myelination and oligodendrogenesis (53). It is not yet understood how these two proteins contribute to myelination gene expression in response to Bace1 deletion, although reduction of myelin basic protein (MBP) and poteolipid protein (PLP) proteins but not their RNA transcripts in P28 and P114 *Bace1*^fl/fl^ and *Bace1*^fl/fl^;*Thy1*-cre mouse hippocampus was noted (Fig. 4B–D). However, hypomyelination with a significant increase in the G ratio irrespective of axon diameter, observed by electron microscopy, was only seen on sciatic nerve sections of 10-month-old *Bace1*^fl/fl^ and *Bace1*^fl/fl^;*Thy1*-cre mice (Fig. 4E and F), but not the corpus callosum axons (data not shown).

Memory deficits in *Bace1*^fl/fl^;*Thy1*-cre mice

Single-nuclear RNAseq results indicated alteration of synaptic pathways in *Bace1*^fl/fl^;*Thy1*-cre mice, and we therefore conducted mouse behavioral tests: open field, Y-maze, Morris water maze and fear conditioning. The open-field test evaluates mouse locomotor activity and anxiety. We found no difference for the total distance traveled in an open arena between *Bace1*^fl/fl^;*Thy1*-cre mice and the age-matched *Bace1*^fl/fl^ controls (Fig. 5A; *P* < 0.05, **P* < 0.01, Student's *t* test). However, *Bace1*^fl/fl^;*Thy1*-cre mice spent increased time in the corners of the open arena compared with controls, likely related to anxiety-like behavior. In the Y-maze, *Bace1*^fl/fl^;*Thy1*-cre mice showed a significant decrease in the total number of arm entries, reflecting
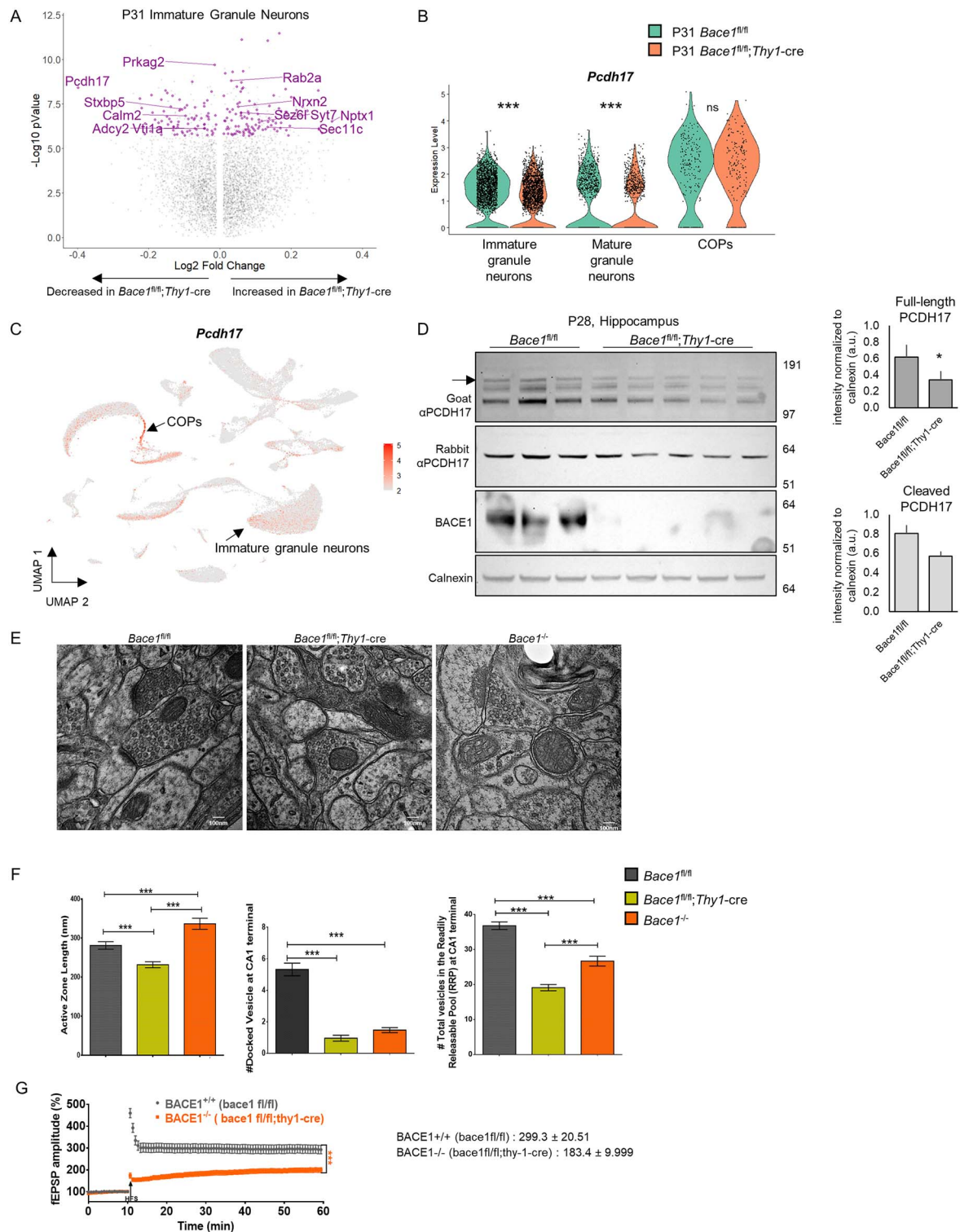
Figure 3. (**A**) Volcano plot of the differentially expressed genes within P31 immature granule neurons between *Bace1*^{fl/fl} and *Bace1*^{fl/fl};*Thy1*-cre mice. Genes labeled in purple are Bonferroni-corrected genes common to male vs male and female vs female comparisons. (**B**) Violin plot of Pcdh17 showing a significant reduction in expression in immature and mature granule neurons of P31 *Bace1*^{fl/fl};*Thy1*-cre mice but not in P31 committed oligodendrocyte progenitors (COPs) (*** = P-value < 0.001). (**C**) Expression of Pcdh17 overlayed onto combined UMAP plots from P31 mice showing highest expression in COPs and immature granule neurons. (**D**, left) Western blot of PCDH17 (full-length, arrow) and c-terminal fragment and BACE1 from P28 *Bace1*^{fl/fl} and *Bace1*^{fl/fl};*Thy1*-cre hippocampal lysates. (D, right) Quantification of full-length and cleaved PCDH17 western blot normalized to calnexin (* = P-value < 0.05). (**E**) Representative electron microscopy images of axonal terminals at the Schaffer collateral:CA1 region from 10-month-old mice. (**F**) Quantification of synapse morphology from electron microscopy (*** = P-value < 0.001). (G) Representative traces from LTP electrophysiology recordings and quantification (*** = P-value < 0.001).
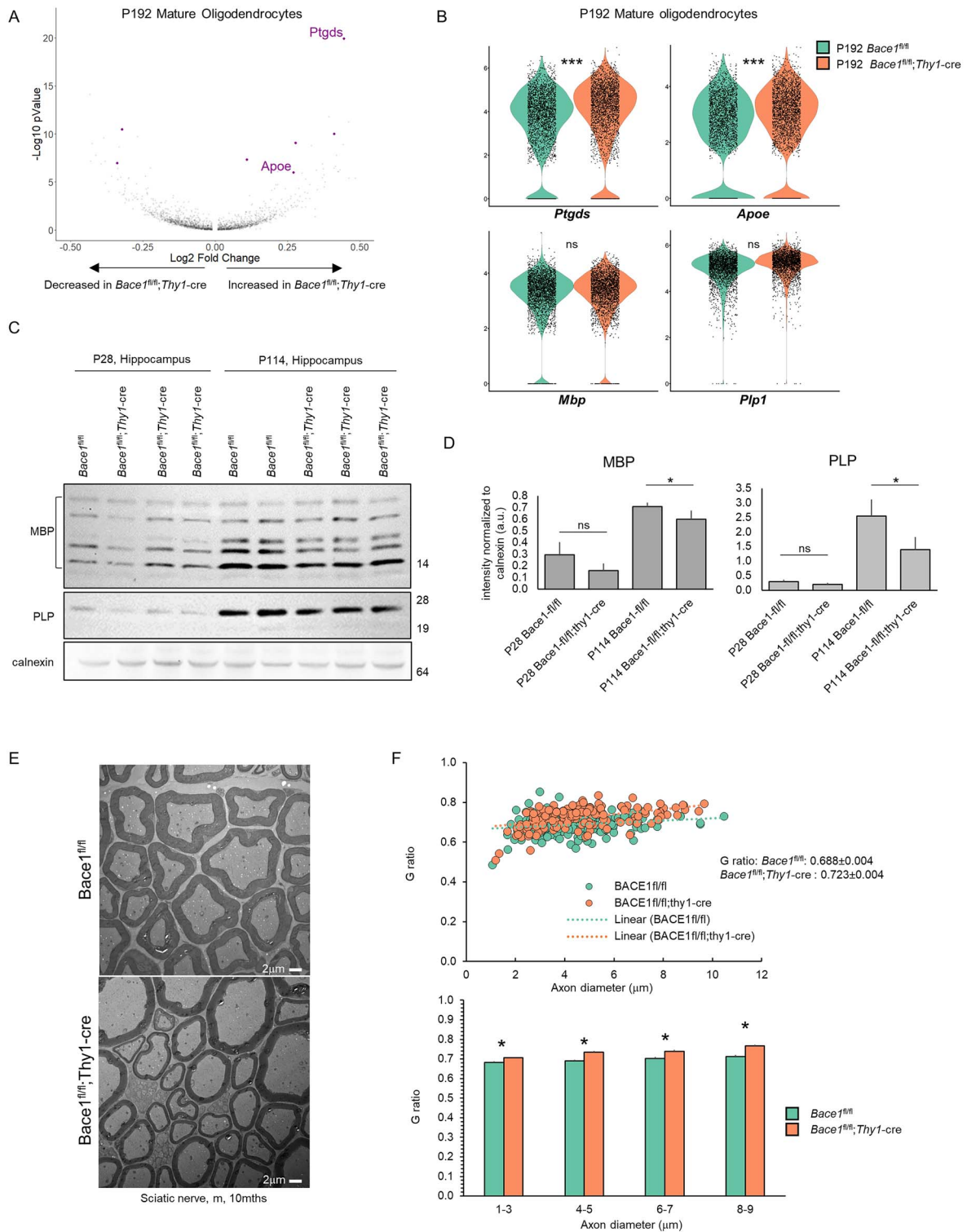
Figure 4. (**A**) Volcano plot showing differentially expressed genes within P192 mature oligodendrocytes between $Bace1^{fl/fl}$ and $Bace1^{fl/fl};Thy1$-cre mice. Genes labeled in purple are Bonferroni-corrected genes common to male vs male and female vs female comparisons. (**B**) Violin plots showing log-normalized expression of $Ptgds$, $Apoe$, Mbp and $Plp1$ within P192 mature oligodendrocytes between $Bace1^{fl/fl}$ and $Bace1^{fl/fl};Thy1$-cre (*** = P-value < 0.001). (**C**) Western blot of MBP and PLP from P28 and P114 $Bace1^{fl/fl}$ and $Bace1^{fl/fl};Thy1$-cre hippocampal lysates. (**D**) Quantification of MBP and PLP western after neuronal deletion of BACE1. (**E**) Representative electron microscopy images from 10-month-old $Bace1^{fl/fl}$ and $Bace1^{fl/fl};Thy1$-cre sciatic nerves. (**F**) Quantification of myelin thickness using G ratio (* = P-value < 0.05).

less exploratory behaviors, and reduced spontaneous alternation compared with age-matched controls (Fig. 5B; *$P < 0.05$, **$P < 0.01$) revealing that BACE1 deletion in neurons causes a spatial working memory deficit.

To test long-term spatial memory, we performed the Morris water maze test, which assesses across four repeated trials and reference memory is determined by preference for the quadrant of the maze when the platform is absent. After 3 days of
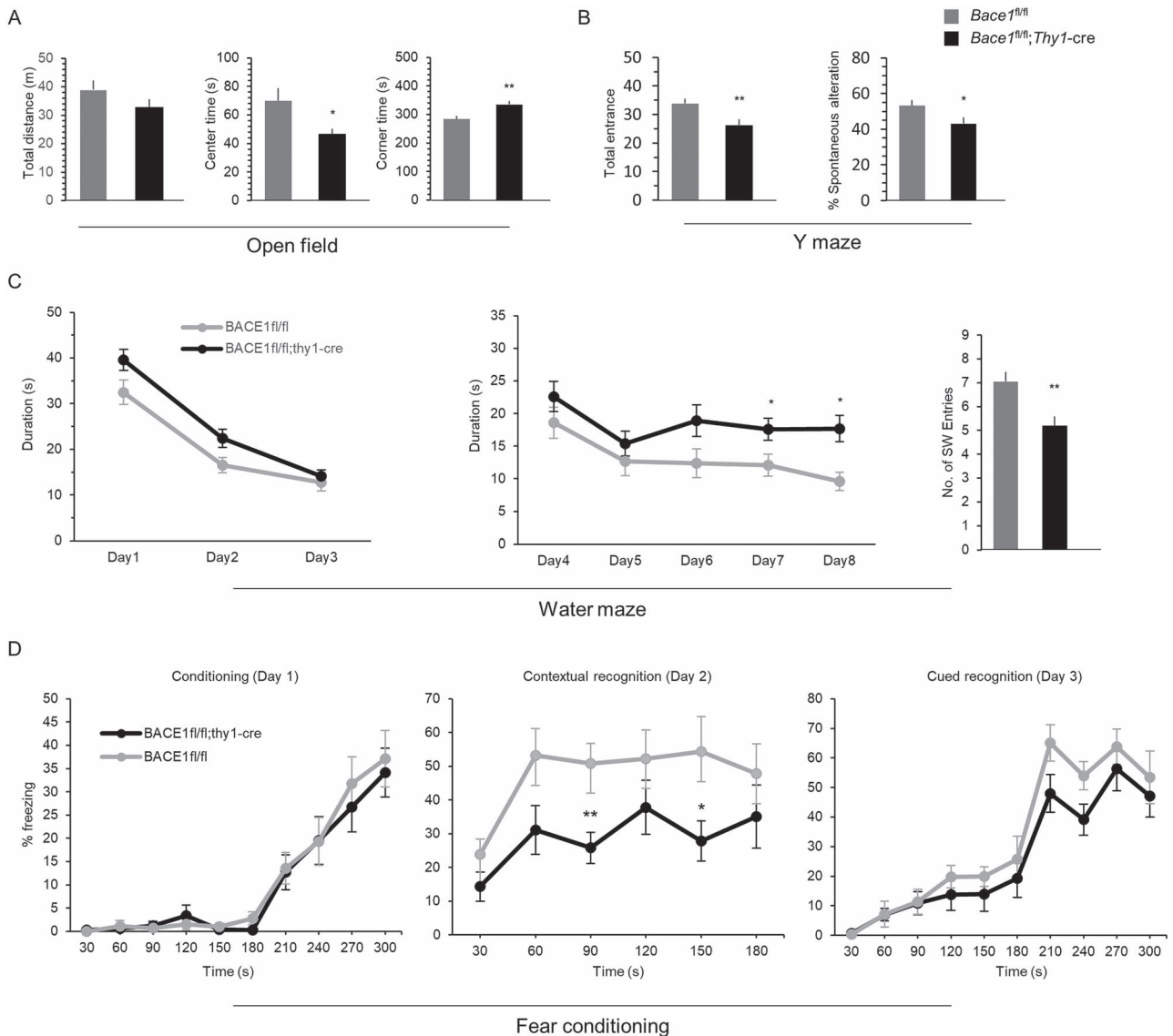
Figure 5. Behavioral assay on 9-month-old *Bace1*^fl/fl and *Bace1*^fl/fl;*Thy1*-cre mice. (**A**) Quantification of total distance traveled in meters, time spent in the center in seconds and time spent in the corners in seconds during the open field behavior test of *Bace1*^fl/fl and *Bace1*^fl/fl;*Thy1*-cre mice. (**B**) Total number of entries during the Y-maze test and the percentage of spontaneous alterations. (**C**) Duration of time in seconds that *Bace1*^fl/fl and *Bace1*^fl/fl;*Thy1*-cre took to reach the platform of the Morris water maze during the first 3 days of habituation and the following days 4–8 (* = P-value < 0.05). (C, right) Quantification of the number of southwest quadrant entries in 30 s after the platform had been removed (** = P-value < 0.01). (**D**, left) Percent time freezing after administration of a 2800 Hz and 85 dB tone for 30 s beginning at 180 s, followed by a 0.5 mA continuous foot shock. (D, middle) Percent context-dependent freezing on day 2 without a tone or foot shock (* = P-value < 0.05, ** = P-value < 0.01). (D, right) Percent freezing to test sound-cued recognition on day 3 where a 2800 Hz and 85 dB tone is administered after 180 s in a novel chamber.

habituation, *Bace1*^fl/fl;*Thy1*-cre mice took a longer time to learn to reach the platform during day 4 to day 8, and the latency to the platform was significantly increased on days 7 and 8 compared with age-matched control. On day 9, the platform was removed, and mice were left in the water maze for 30 s to test probe capability. The number of entries made to the platform quadrant was significantly reduced in *Bace1*^fl/fl;*Thy1*-cre compared with age-matched controls (Fig. 5C; *P < 0.05, **P < 0.01), revealing that *Bace1*^fl/fl;*Thy1*-cre mice also exhibited deficits in spatial learning and reference memory.

Lastly, we conducted fear conditioning test to assess animal learning and memory. During this test, the associative learning of a cue (sound) or a context (environment) with a brief aversive stimulus (electric shock) was measured by

analyzing the freezing response of mice. On day 1 test, the mice were placed in the fear conditioning chamber and exposed to a sound followed by a foot shock. Both *Bace1*^fl/fl;*Thy1*-cre and the control mice had similar levels of freezing. Context-dependent freezing was recorded on day 2 by placing mice back in the same chamber but without exposure to the sound or shock. *Bace1*^fl/fl;*Thy1*-cre mice exhibited a lower freezing time (Fig. 5D; *P < 0.05, **P < 0.01), indicating that deletion of BACE1 in neurons impaired contextual fear learning. On day 3 test, the freezing time of mice in response to the sound in a context-altered chamber was unchanged between the groups. Together, we found that *Bace1*^fl/fl;*Thy1*-cre mice have many impaired cognitive behaviors that are seen in *Bace1*-null mice (Table 1).

Table 1. Comparison of behavioral phenotypes due to *Bace1* deletion by cell type

Mouse line	Cell type specificity	Open field	Y-Maze	Water maze	Fear conditioning	LTP	Ref
Bace1$^{-/-}$	Global deletion	Increased travel distance, increased center time	Decreased spontaneous alternation	Deficit	N/A	Deficit	(18,50,54)
Bace1$^{fl/fl}$; R26CreER^{T2} + TAM	Postnatal global deletion	No change	Increased arm entries	No change	No change	No change	(55)
Bace1$^{fl/fl}$;R26Cre-ERT2$^{+/WT}$ + TAM	Partial postnatal global deletion	No change	No change	No change	No change	Deficit	(56)
Bace1$^{fl/fl}$;Ubc-Cre	Postnatal global deletion	N/A	N/A	N/A	No change	Deficit	(11)
Bace1$^{fl/fl}$;Camk2α-iCre	Early postnatal forebrain neuron	Increased travel distance	Increased arm entries	No change	No change	No change	(55)
Bace1$^{fl/fl}$;Thy1-Cre	Postnatal forebrain neuron	Increased corner time	Decreased arm entries, decreased spontaneous alternation	Deficit	Deficit	Deficit	

Discussion

In this study, we aim to characterize the effect of neuronal BACE1 deletion on the transcriptome of P31 and P192 CNS cell types using single-nuclear RNA sequencing on the hippocampi of eight animals (Fig. 1C). This technique allowed us to detect a shift in the abundance of neuroblasts and oligodendrocytes, which suggested a developmental delay in neuronal maturation and oligodendrocyte maturation (Fig. 1E). Using RNA velocity and differential gene expression analysis, neuronal BACE1 deletion had its largest effect on immature granule neurons of the hippocampus. Of these differentially expressed genes, we identified a reduction in *Pcdh17* expression, a recently identified BACE1 target that plays a role in synaptic function (Fig. 3A and B) (42). We confirmed reduction of PCDH17 protein and a likely BACE1-cleaved product (Fig. 3C and D). Pathway analysis of the differentially expressed genes within immature granule neurons suggested a deficit in synaptic function, which was confirmed by using electron microscopy imaging of the synapse, electrophysiology and behavioral tests (Figs 3 and 5). Together, we showed that deletion of neuronal Bace1 would recapture many phenotypes seen Bace1-null mice.

An intriguing and novel result was a deficit in the abundance of oligodendrocytes and their ability to properly myelinate axons after neuronal BACE1 deletion (Fig. 4). Previous reports postulated neuregulin 1 as a neuronal BACE1 substrate that influences myelination (20,21). Unbiased snRNAseq results revealed PCDH17 as another potential contributor to myelination defects. During neuronal development, neuronal PCDH17 recruits the actin polymerization regulatory complex WAVE to direct axonal maturation (49), and the initiation of oligodendrocyte process extension also requires this regulatory complex (57,58). A recent study has identified *Pcdh17* expression in immature oligodendrocytes along with a long non-coding RNA in *Pcdh17* exon 1, *Pcdh17it*, and found PCDH17 to initiate myelination through regulating *f*-actin (59). *Pcdh17* is expressed at a high level in COPs as well as immature granule neurons (Fig. 3B), in line with transcellular communication of Pcdh17 between immature neurons and immature oligodendrocytes via BACE1 regulation for initiating both axonal extension and myelination. Other BACE1 substrates such as CHL1, NRG1 and APP increase in their protein level due to loss of proteolytic processing. Interestingly, we observe transcriptomic changes in BACE1 substrates such as *Chl1*, but it is not significant

in all samples and ages (Supplementary Material, Table S1). We show a consistent reduction in PCDH17 at the mRNA and protein level in response to neuronal BACE1 deletion; however, we suspect that increase in protein and regulation at the mRNA level are the result of direct and indirect BACE1 signaling, respectively. We speculate there is additional signaling leading to PCDH17 regulation at the transcriptomic level that results in decreased total protein in neurons. We have shown PCDH17 is expressed highly in oligodendrocyte progenitor cells and is unaffected by BACE1 KO in neurons which could be masking neuron specific changes to PCDH17. Use of techniques that investigate protein changes at single-cell resolution is critical to understanding the role of BACE1 in this context (60).

Deletion of Bace1 via *CamK2α*-cre mouse line appears to cause reduced length and disorganization of the hippocampal mossy fiber infrapyramidal bundle while spares most of development-related phenotypes (55). CamK2α promoter drives Cre expression mainly in the forebrain (61), while Thy-1 promoter drives expression of Cre expression more broad brain regions and peripheral sciatic nerves (62). Cre recombinase activity was detected in immature proliferative zones as early as embryonic day 11 in Thy-1-cre mice, although strong Cre activity is expected in postmitotic neurons (62). Observing more severe phenotypes in *Bace1*$^{fl/fl}$;*Thy1*-cre mice than in *Bace1*$^{fl/fl}$;*CamK2a*-cre mice reinforce the important role of BACE1 in neurons, and this is consistent with the increased ventricular regions in BACE1 inhibitors observed in human trials (63). It is interesting to speculate the effect of hemizygous *Bace1* knockout on neuroblast maturation using a *Bace1*$^{fl/+}$;*Thy1*-cre mouse. A partial loss in BACE1 activity may be sufficient to reduce the generation of amyloid pathology but still retain normal synaptic function. Given BACE1 critical function in neuronal and synaptic maturation, drastic inhibition of BACE1 in neurons should be avoided in future development of BACE1 inhibitors for AD treatment, aiming to modulate its function to a lesser degree.

Materials and Methods
Animals

BACE1$^{fl/fl}$ mice were bred with Tg (Thy1-cre) mice (006143; Jackson Laboratory) to obtain mice heterozygous for the transgenic Cre and homozygous for the floxed BACE1 (*BACE1*$^{fl/fl}$;Thy1-cre) mice.

Both lines were routinely backcrossed with C57BL/6 J mice for at least five generations to ensure consistent genetic background for phenotypic analyses. All animal use and procedures were performed according to the Institutional Animal Care and Use protocols at UConn Health, Farmington, and in compliance with the guidelines established by the Guide for the Care and Use of Laboratory Animals, as adopted by the National Institutes of Health. Nine month-old mice were used in all behavioral tests: 11 female and 11 male of *Bace1*^fl/fl^; 8 female and 14 male of *Bace1*^fl/fl^;*Thy1*-cre.

Single nuclear transcript generation

Eight hippocampi from P31 and P192 male and female *Bace1*^fl/fl^ and *Bace1*^fl/fl^;*Thy1*-cre mice were extracted and snap-frozen on dry ice. Hippocampi were then homogenized and lysed in buffer containing 0.01% tween/0.01% NP-40 on ice. Debris removal (Miltenyi) step was included to remove myelin debris, and nuclei were counted and loaded onto a droplet-based 10x Chromium controller to perform single-cell partitioning and barcoding. Raw sequencing from the NovaSeq6000 was aligned and annotated using the CellRanger v3.1.0 pipeline. During FASTQ generation, reads with more than 1 mismatch in the 8 bp i7 index were excluded. During alignment using STAR (64), only reads with MAPQ scores greater than 255 aligned to annotated transcripts were retained. Reads containing bases with Q30 scores below 3 were also excluded. After alignment, cell barcodes were filtered up to 1 mismatch against a whitelist of 737 500 barcodes provided by 10X Genomics. Barcodes associated with cells were distinguished from ambient mRNA using an adaptively computed UMI threshold. The raw count matrix was filtered using cutoff values of mitochondrial transcripts below 5% and between 250 and 6000 unique features.

Dimensionality reduction and clustering

The expression profiles of each cell using the 2000 most variable genes as measured by dispersion (65,66) were used for neighborhood graph generation and dimensionality reduction with UMAP [McInnis 2020 arXiv:1802.03426]. Clustering was performed on this neighborhood graph using the Leiden community detection algorithm (67). Because the experiments consisted of multiple samples, the neighborhood graph was batch-corrected using the batch correction software BBKNN (68). Subclustering and differential expression were performed ad hoc on a per-cluster basis using the Seurat R toolkit v4.0 (69).

Calculating spliced and unspliced RNA reads

To calculate the spliced and unspliced mRNAs from our single-nuclear RNA sequencing data, we utilized the python package velocyto.py (https://github.com/velocyto-team/velocyto.py) in which short reads were aligned to the mm10 mouse reference genome (ensemble.org) (38).

RNA velocity

RNA velocity was performed using the scvelo python package (https://github.com/theislab/scvelo). Briefly, we combined the outputs of velocyto into P31 and P192 *Bace1*^fl/fl^ and *Bace1*^fl/fl^;*Thy1*-cre (one male and one female per age and genotype). Gene ranking was completed using a differential expression test (Welch t-test) on velocity expression, to find genes within cell types that show dynamics transcriptionally regulated differently compared to all other cell types. Terminal states (root and end points) were obtained as stationary states of the velocity-inferred transition matrix. Velocity-pseudotime was

calculated by inferring a distribution over the root cells from the velocity-inferred transition matrix and then computing distances from diffusion random walks on the velocity graph.

Immunohistochemistry

Animals were euthanized and brains were surgically removed and cut mid-sagittally into equal half of brains. One half was fixed in 4% paraformaldehyde for 24 h and immersed in 20% sucrose overnight at 4°C. Brains were sectioned sagittally (14–16 μm thick) on a cryostat microtome (Thermo HM525 NX). Sections on the slides were washed in PBS 3× for 5 min to remove OCT and then permeabilized with 0.3% Triton X-100 for 30 min, followed by washing with PBS (3× for 5 min). Antigen retrieval was performed by microwaving the sections in 0.05 M citrate-buffered saline (pH 6.0) for 3 min. The sections were blocked with 5% normal goat serum and incubated with the following primary antibodies at 1:1000 dilution: NeuN (Chemicon, MAB377), Dcx (Cell Signaling, 4604) and SMI22 (Covance, SMI-22R). After washing with PBS (3× for 5 min), sections were incubated with Alexa Fluor-conjugated secondary antibody (1:400 in blocking buffer) at room temperature (RT) for 2 h. Slides were washed three times in PBS and mounted on a coverslip with Antifade Mounting Medium.

Protein isolation and Western blotting

Hippocampi isolated from *Bace1*^fl/fl^;*Thy1*-cre and *Bace1*^fl/fl^ littermates were lysed on ice in RIPA lysis buffer containing 50 mM Tris–HCl (pH 7.4), 1 mM EDTA, 100 mM NaCl and 0.1% SDS. The lysate was collected and further sonicated on ice for 30 s on and off cycle for 5 min and then centrifuged at 15 000 × *g* for 15 min at 4°C. Protein concentrations were determined using a BCA assay kit (Pierce). Equal amounts of protein from each sample were loaded and electrophoretically resolved on 4–12% SDS-PAGE (NuPAGE system, Life Technologies) gels. After electrophoresis, proteins were transferred to nitrocellulose membranes at 100 V for 2 h. The membranes were blocked with 5% bovine serum albumin (BSA) for 1 h at room temperature. The membranes were probed with primary antibody (1: 1000 dilution), followed by incubation with secondary HRP-conjugated antibody (1:1000). The antibody-bound proteins were detected by iBright 1500 imaging system (Invitrogen). To ensure equal loading, the blots were re-probed with monoclonal anti-actin (1:1000) or calnexin (1:1000). For quantification purposes, band intensities of immunoblots were analyzed using image J software.

Antibodies

Antibody name	Catalog no.	RRID	Manufacturer
NeuN	MAB377	AB_2298772	Chemicon
Dcx	4604	AB_561007	Cell Signaling
SMI22	SMI-22R	AB_2314542	Covance
BACE1			Gift from XiaoXin lab
Actin	A5441	AB_476744	Sigma
MBP	SMI-94	AB_510039	Sternberger Monoclonals
PLP	AA3		Gift from Trapp Lab
Pcdh17	ab128815	AB_11144709	Abcam
Pcdh17	A10512	AB_2758062	ABclonal
Calnexin	C4731	AB_476845	Sigma

Electron microscopy and quantification

The mice were perfused transcardially with 20 ml of 0.1 M phosphate buffer (PB, pH 7.2) followed by 150 ml of fixative solution for 15 min containing 4% paraformaldehyde and 2.5% glutaraldehyde in 0.1 M PB. Brains were postfixed with fresh fixative overnight and 100 μm coronal sections were obtained on a vibratome (Campden 7000smz-2). Sections were rinsed with 0.1 M sodium cacodylate buffer, postfixed with 1% osmium tetroxide, 1.5% potassium ferrocyanide in 0.1 M sodium cacodylate buffer, en bloc stained with aqueous 1% uranyl acetate and dehydrated in ethanol. Following infiltration in resin tissue was embedded in Poly/Bed 812 and polymerized at 60°C for 48 h. Ultrathin sections (70 nm) were stained with 6% methanolic uranyl acetate and lead citrate and examined in a Hitachi H-7650 transmission electron microscope operating at 80 kV. Images used for quantification were taken at ×30,000 magnification with AMT camera and software.

Quantification of G-ratios

The myelinated axon circumference was measured by digitally tracing the inner and outer layers of the myelinated fiber using ImageJ software. The G-ratio was calculated by dividing the inner circumference of the axon (without myelin) by the outer circumference of the total fiber (including myelin). Three pairs of *Bace1*$^{fl/fl}$;*Thy1*-cre and *Bace1*$^{fl/fl}$ mice were processed for the quantification of G-ratios.

Electrophysiology

LTP recordings on hippocampal slices were performed according to previously described procedures (50). Upon obtaining horizontal hippocampal slices from the brains of mice, the prepared slices were then placed onto the center of an MED probe (MED-P515A; AutoMate Scientific) with continuous perfusion of aCSF and bubbling of 95% O_2 and 5% CO_2. The device has an array arranged in an 8 × 8 pattern of 64 planar microelectrodes across a hippocampal slice. Each electrode is 20 × 20 μm with an inter-electrode distance of 150 μm. A MED-A64HE1S head amplifier and a MED-A64MD1 main amplifier, run by Mobius software, were used for data acquisition and analysis. Schaffer collateral (SCs) to CA1 synapses were typically analyzed for LTP assays. Field excitatory post synaptic potentials (fEPSPs) caused by stimulation were recorded at a 20-kHz sampling rate within the CA1 subregion of the hippocampus. Control fEPSPs were recorded for at least 10 min before the conditioning stimulation, using a response ~50% of the maximum. After a stable baseline was established, LTP was induced with three trains of 100 Hz for 1 s with an intertrain interval of 20 s. Field potential amplitudes were then measured. Data are expressed as mean ± SEM. Synaptic strength was evaluated by measuring changes in the fEPSP amplitude relative to baseline. Six *Bace1*$^{fl/fl}$ and six *Bace1*$^{fl/fl}$;*Thy1*-cre mice were used for this experiment. Statistics were calculated using Student's *t* tests.

Open field

Open field is often used to assess animal hyperactivity, exploratory behaviors and anxiety. The square acrylic open-field arena (San Diego Instruments) is 20 in long, 20 in wide and 15 in high. Each mouse was released in the middle of the arena and 10 min of free exploration was recorded via ANY-maze video tracking system. Activity measures included distance traveled, time spent in corners vs in the center of the arena and speed of movement during active exploration.

Y-maze

Y-maze is commonly used to evaluate animal spatial working memory that is dependent upon the hippocampus. The symmetrical Y-maze (San Diego Instruments) made of acrylic consists of three arms separated by 120°. Each arm is 15 in long, 5 in high and 3 in wide. Each mouse was placed in the center of the Y-maze and was allowed to explore freely through the maze during a 5 min session. The sequence and total number of arms entered was recorded via ANY-maze video tracking system. Arm entry was completed when half mouse body had been completely placed in the arm. Percentage of alternations is the number of triads containing entries into all three arms divided by the maximum possible alternations (the total number of arms entered − 2) × 100.

Morris water maze

Morris water maze is the most widely used to assess spatial learning and reference memory. The apparatus consisted of a white circular tank (48 in in diameter and 32 in deep) filled with water (22°C). The water was made to appear opaque using white nontoxic paint. A transparent platform (4 in in diameter) was in the middle of the southwest quadrant. Mice were subjected to four consecutive trials each day over a 3-day training period (with a flag attached to the platform and the surface of platform was 0.5 cm above the water) and then 5-day reference memory test (no flag attached to the platform and the surface of platform was submerged 0.5 cm below the water). Each mouse was released from four different positions around the perimeter of the tank (west, north, east, south). In each trial, the mouse was allowed to swim until it found the platform (for a maximum of 60 s) and was subsequently left on the platform for 20 s. If the platform was not found in 60 s, the mouse was guided to the platform and remained there for 20 s. The escape latency to find the hidden platform was automatically recorded via ANY-maze video tracking system (San Diego instruments). A probe test was conducted for 30 s on the ninth day. The platform was removed. Each mouse was released from the east point and was allowed to swim for 30 s. Memory retention was measured by quantifying time spent and number of entries in the target quadrant (southwest quadrant).

Contextual fear conditioning test

The standard contextual fear conditioning test is conducted over 3 days. On the first day, which was the conditioning period, the mouse was placed in the conditioning chamber (Med Associates) for 3 min (phase A) before the onset of the sound at 2800 Hz and 85 dB for 30 s (phase B, conditioning stimulus). The last 2 s of the conditioning stimulus was coupled with a 0.5 mA continuous foot shock (phase C, unconditioned stimulus). After resting an additional 30 s in the chamber, phases B and C were repeated once, and the mouse was returned to its home cage after resting in the chamber for 30 s. On the second day, mice were tested for their contextual memory in the same chamber for 3 min without either sound or foot shock. On the third day, mice were tested for tone memory in a different chamber environment for 5 min with the sound but no foot shock. Fear memory was measured as the percentage of freezing, which was defined as the percentage of time completely lacking movement, except for respiration, in intervals of 1 s.

Statistical analysis

Results with statistical significance are expressed as mean ± SEM with *$P < 0.05$, **$P < 0.01$, ***$P < 0.001$ using Student's t-test. The statistical calculation was using GraphPad Prism 6.0 software

(GraphPad Software, San Diego). Differential gene expression between conditions in single-nuclear RNAseq data set was analyzed using MAST (Model-based Analysis of Single-cell Transcriptomics) (47). Gene ranking comparing RNA velocity between samples was completed using a differential expression test (Welch t-test).

Data availability

GSE217960.

Supplementary Material

Supplementary Material is available at HMG online.

Acknowledgements

Funding

Authors' contributions

M.B. and X.H. isolated tissues for snRNAseq and M.B. performed the analysis. B.D. and A.Y. performed electrophysiology experiments. X.H. and Y.G. performed the behavioral experiments. M.D., M.B. and X.H performed western blotting. M.B., R.Y. and X.H. wrote the manuscript.

References

1. Selkoe, D.J. and Hardy, J. (2016) The amyloid hypothesis of Alzheimer's disease at 25 years. *EMBO Mol. Med.*, **8**, 595–608.
2. Rahman, M.M. and Lendel, C. (2021) Extracellular protein components of amyloid plaques and their roles in Alzheimer's disease pathology. *Mol. Neurodegener.*, **16**, 59.
3. Long, J.M. and Holtzman, D.M. (2019) Alzheimer disease: an update on pathobiology and treatment strategies. *Cell*, **179**, 312–339.
4. Cummings, J. (2021) New approaches to symptomatic treatments for Alzheimer's disease. *Mol. Neurodegener.*, **16**, 2.
5. Tanzi, R.E., Gusella, J.F., Watkins, P.C., Bruns, G.A., St George-Hyslop, P., Van Keuren, M.L., Patterson, D., Pagan, S., Kurnit, D.M. and Neve, R.L. (1987) Amyloid beta protein gene: cDNA, mRNA distribution, and genetic linkage near the Alzheimer locus. *Science*, **235**, 880–884.
6. Haass, C., Kaether, C., Thinakaran, G. and Sisodia, S. (2012) Trafficking and proteolytic processing of APP. *Cold Spring Harb. Perspect. Med.*, **2**, a006270.
7. Yan, R., Bienkowski, M.J., Shuck, M.E., Miao, H., Tory, M.C., Pauley, A.M., Brashier, J.R., Stratman, N.C., Mathews, W.R., Buhl, A.E. *et al.* (1999) Membrane-anchored aspartyl protease with Alzheimer's disease beta-secretase activity. *Nature*, **402**, 533–537.
8. Vassar, R., Bennett, B.D., Babu-Khan, S., Kahn, S., Mendiaz, E.A., Denis, P., Teplow, D.B., Ross, S., Amarante, P., Loeloff, R. *et al.* (1999) Beta-secretase cleavage of Alzheimer's amyloid precursor protein by the transmembrane aspartic protease BACE. *Science*, **286**, 735–741.
9. Sinha, S., Anderson, J.P., Barbour, R., Basi, G.S., Caccavello, R., Davis, D., Doan, M., Dovey, H.F., Frigon, N., Hong, J. *et al.* (1999) Purification and cloning of amyloid precursor protein beta-secretase from human brain. *Nature*, **402**, 537–540.
10. Luo, Y., Bolon, B., Kahn, S., Bennett, B.D., Babu-Khan, S., Denis, P., Fan, W., Kha, H., Zhang, J., Gong, Y. *et al.* (2001) Mice deficient in BACE1, the Alzheimer's beta-secretase, have normal phenotype and abolished beta-amyloid generation. *Nat. Neurosci.*, **4**, 231–232.
11. Hu, X., Das, B., Hou, H., He, W. and Yan, R. (2018) BACE1 deletion in the adult mouse reverses preformed amyloid deposition and improves cognitive functions. *J. Exp. Med.*, **215**, 927–940.
12. Cai, H., Wang, Y., McCarthy, D., Wen, H., Borchelt, D.R., Price, D.L. and Wong, P.C. (2001) BACE1 is the major beta-secretase for generation of Abeta peptides by neurons. *Nat. Neurosci.*, **4**, 233–234.
13. Hemming, M.L., Elias, J.E., Gygi, S.P. and Selkoe, D.J. (2009) Identification of beta-secretase (BACE1) substrates using quantitative proteomics. *PLoS One*, **4**, e8477.
14. Kuhn, P.-H., Koroniak, K., Hogl, S., Colombo, A., Zeitschel, U., Willem, M., Volbracht, C., Schepers, U., Imhof, A., Hoffmeister, A. *et al.* (2012) Secretome protein enrichment identifies physiological BACE1 protease substrates in neurons. *EMBO J.*, **31**, 3157–3168.
15. Hampel, H., Vassar, R., De Strooper, B., Hardy, J., Willem, M., Singh, N., Zhou, J., Yan, R., Vanmechelen, E., De Vos, A. *et al.* (2021) The β-secretase BACE1 in Alzheimer's disease. *Biol. Psychiatry*, **89**, 745–756.
16. Dominguez, D., Tournoy, J., Hartmann, D., Huth, T., Cryns, K., Deforce, S., Serneels, L., Camacho, I.E., Marjaux, E., Craessaerts, K. *et al.* (2005) Phenotypic and biochemical analyses of BACE1- and BACE2-deficient mice. *J. Biol. Chem.*, **280**, 30797–30806.
17. Cheret, C., Willem, M., Fricker, F.R., Wende, H., Wulf-Goldenberg, A., Tahirovic, S., Nave, K.-A., Saftig, P., Haass, C., Garratt, A.N. *et al.* (2013) Bace1 and Neuregulin-1 cooperate to control formation and maintenance of muscle spindles. *EMBO J.*, **32**, 2015–2028.
18. Laird, F.M., Cai, H., Savonenko, A.V., Farah, M.H., He, K., Melnikova, T., Wen, H., Chiang, H.-C., Xu, G., Koliatsos, V.E. *et al.* (2005) BACE1, a major determinant of selective vulnerability of the brain to amyloid-beta amyloidogenesis, is essential for cognitive, emotional, and synaptic functions. *J. Neurosci.*, **25**, 11693–11709.
19. Ohno, M., Chang, L., Tseng, W., Oakley, H., Citron, M., Klein, W.L., Vassar, R. and Disterhoft, J.F. (2006) Temporal memory deficits in Alzheimer's mouse models: rescue by genetic deletion of BACE1. *Eur. J. Neurosci.*, **23**, 251–260.
20. Willem, M., Garratt, A.N., Novak, B., Citron, M., Kaufmann, S., Rittger, A., DeStrooper, B., Saftig, P., Birchmeier, C. and Haass, C. (2006) Control of peripheral nerve myelination by the beta-secretase BACE1. *Science*, **314**, 664–666.
21. Hu, X., Hicks, C.W., He, W., Wong, P., Macklin, W.B., Trapp, B.D. and Yan, R. (2006) Bace1 modulates myelination in the central and peripheral nervous system. *Nat. Neurosci.*, **9**, 1520–1525.
22. Hu, X., He, W., Diaconu, C., Tang, X., Kidd, G.J., Macklin, W.B., Trapp, B.D. and Yan, R. (2008) Genetic deletion of BACE1 in mice affects remyelination of sciatic nerves. *FASEB. J.*, **22**, 2970–2980.
23. Hu, X., Zhou, X., He, W., Yang, J., Xiong, W., Wong, P., Wilson, C.G. and Yan, R. (2010) BACE1 deficiency causes altered neuronal activity and neurodegeneration. *J. Neurosci.*, **30**, 8819–8829.
24. Hitt, B.D., Jaramillo, T.C., Chetkovich, D.M. and Vassar, R. (2010) BACE1−/− mice exhibit seizure activity that does not correlate

with sodium channel level or axonal localization. *Mol. Neurodegener.*, **5**, 31.

25. Rajapaksha, T.W., Eimer, W.A., Bozza, T.C. and Vassar, R. (2011) The Alzheimer's β-secretase enzyme BACE1 is required for accurate axon guidance of olfactory sensory neurons and normal glomerulus formation in the olfactory bulb. *Mol. Neurodegener.*, **6**, 88.

26. Hitt, B., Riordan, S.M., Kukreja, L., Eimer, W.A., Rajapaksha, T.W. and Vassar, R. (2012) β-Site amyloid precursor protein (APP)-cleaving enzyme 1 (BACE1)-deficient mice exhibit a close homolog of L1 (CHL1) loss-of-function phenotype involving axon guidance defects. *J. Biol. Chem.*, **287**, 38408–38425.

27. Cao, L., Rickenbacher, G.T., Rodriguez, S., Moulia, T.W. and Albers, M.W. (2012) The precision of axon targeting of mouse olfactory sensory neurons requires the BACE1 protease. *Sci. Rep.*, **2**, 231.

28. Barão, S., Gärtner, A., Leyva-Díaz, E., Demyanenko, G., Munck, S., Vanhoutvin, T., Zhou, L., Schachner, M., López-Bendito, G., Maness, P.F. *et al.* (2015) Antagonistic effects of BACE1 and APH1B-γ-secretase control axonal guidance by regulating growth cone collapse. *Cell Rep.*, **12**, 1367–1376.

29. Yan, R. and Vassar, R. (2014) Targeting the β secretase BACE1 for Alzheimer's disease therapy. *Lancet Neurol.*, **13**, 319–329.

30. Singh, N., Benoit, M.R., Zhou, J., Das, B., Davila-Velderrain, J., Kellis, M., Tsai, L.-H., Hu, X. and Yan, R. (2022) BACE-1 inhibition facilitates the transition from homeostatic microglia to DAM-1. *Sci. Adv.*, **8**, eabo1286.

31. Dewachter, I., Reversé, D., Caluwaerts, N., Ris, L., Kuipéri, C., Van den Haute, C., Spittaels, K., Umans, L., Serneels, L., Thiry, E. *et al.* (2002) Neuronal deficiency of presenilin 1 inhibits amyloid plaque formation and corrects hippocampal long-term potentiation but not a cognitive defect of amyloid precursor protein [V717I] transgenic mice. *J. Neurosci.*, **22**, 3445–3453.

32. Bakken, T.E., Hodge, R.D., Miller, J.A., Yao, Z., Nguyen, T.N., Aevermann, B., Barkan, E., Bertagnolli, D., Casper, T., Dee, N. *et al.* (2018) Single-nucleus and single-cell transcriptomes compared in matched cortical cell types. *PLoS One*, **13**, e0209648.

33. Wang, M., Song, W.-M., Ming, C., Wang, Q., Zhou, X., Xu, P., Krek, A., Yoon, Y., Ho, L., Orr, M.E. *et al.* (2022) Guidelines for bioinformatics of single-cell sequencing data analysis in Alzheimer's disease: review, recommendation, implementation and application. *Mol. Neurodegener.*, **17**, 17.

34. Alić, I., Kosi, N., Kapuralin, K., Gorup, D., Gajović, S., Pochet, R. and Mitrečić, D. (2016) Neural stem cells from mouse strain Thy1 YFP-16 are a valuable tool to monitor and evaluate neuronal differentiation and morphology. *Neurosci. Lett.*, **634**, 32–41.

35. Kriegstein, A. and Alvarez-Buylla, A. (2009) The glial nature of embryonic and adult neural stem cells. *Annu. Rev. Neurosci.*, **32**, 149–184.

36. Gage, F.H. (2019) Adult neurogenesis in mammals. *Science*, **364**, 827–828.

37. Hochgerner, H., Zeisel, A., Lönnerberg, P. and Linnarsson, S. (2018) Conserved properties of dentate gyrus neurogenesis across postnatal development revealed by single-cell RNA sequencing. *Nat. Neurosci.*, **21**, 290–299.

38. La Manno, G., Soldatov, R., Zeisel, A., Braun, E., Hochgerner, H., Petukhov, V., Lidschreiber, K., Kastriti, M.E., Lönnerberg, P., Furlan, A. *et al.* (2018) RNA velocity of single cells. *Nature*, **560**, 494–498.

39. Bergen, V., Lange, M., Peidli, S., Wolf, F.A. and Theis, F.J. (2020) Generalizing RNA velocity to transient cell states through dynamical modeling. *Nat. Biotechnol.*, **38**, 1408–1414.

40. Hou, H., Fan, Q., He, W., Suh, H., Hu, X. and Yan, R. (2017) BACE1 deficiency causes abnormal neuronal clustering in the dentate gyrus. *Stem Cell Rep.*, **9**, 217–230.

41. Pigoni, M., Wanngren, J., Kuhn, P.-H., Munro, K.M., Gunnersen, J.M., Takeshima, H., Feederle, R., Voytyuk, I., De Strooper, B., Levasseur, M.D. *et al.* (2016) Seizure protein 6 and its homolog seizure 6-like protein are physiological substrates of BACE1 in neurons. *Mol. Neurodegener.*, **11**, 67.

42. Taylor, H.A., Simmons, K.J., Clavane, E.M., Trevelyan, C.J., Brown, J.M., Przemyłska, L., Watt, N.T., Matthews, L.C. and Meakin, P.J. (2022) PTPRD and DCC are novel BACE1 substrates differentially expressed in Alzheimer's disease: a data mining and bioinformatics study. *Int. J. Mol. Sci.*, **23**, 4568.

43. Faivre-Sarrailh, C. and Rougon, G. (1997) Axonal molecules of the immunoglobulin superfamily bearing a GPI anchor: their role in controlling neurite outgrowth. *Mol. Cell. Neurosci.*, **9**, 109–115.

44. Rougon, G. and Hobert, O. (2003) New insights into the diversity and function of neuronal immunoglobulin superfamily molecules. *Annu. Rev. Neurosci.*, **26**, 207–238.

45. Gunnersen, J.M., Kim, M.H., Fuller, S.J., De Silva, M., Britto, J.M., Hammond, V.E., Davies, P.J., Petrou, S., Faber, E.S.L., Sah, P. *et al.* (2007) Sez-6 proteins affect dendritic arborization patterns and excitability of cortical pyramidal neurons. *Neuron*, **56**, 621–639.

46. Nash, A., Aumann, T.D., Pigoni, M., Lichtenthaler, S.F., Takeshima, H., Munro, K.M. and Gunnersen, J.M. (2020) Lack of Sez6 family proteins impairs motor functions, short-term memory, and cognitive flexibility and alters dendritic spine properties. *Cereb. Cortex*, **30**, 2167–2184.

47. Finak, G., McDavid, A., Yajima, M., Deng, J., Gersuk, V., Shalek, A.K., Slichter, C.K., Miller, H.W., McElrath, M.J., Prlic, M. *et al.* (2015) MAST: a flexible statistical framework for assessing transcriptional changes and characterizing heterogeneity in single-cell RNA sequencing data. *Genome Biol.*, **16**, 278.

48. Hayashi, S., Inoue, Y., Kiyonari, H., Abe, T., Misaki, K., Moriguchi, H., Tanaka, Y. and Takeichi, M. (2014) Protocadherin-17 mediates collective axon extension by recruiting actin regulator complexes to interaxonal contacts. *Dev. Cell*, **30**, 673–687.

49. Hoshina, N., Tanimura, A., Yamasaki, M., Inoue, T., Fukabori, R., Kuroda, T., Yokoyama, K., Tezuka, T., Sagara, H., Hirano, S. *et al.* (2013) Protocadherin 17 regulates presynaptic assembly in topographic corticobasal Ganglia circuits. *Neuron*, **78**, 839–854.

50. Das, B., Singh, N., Yao, A.Y., Zhou, J., He, W., Hu, X. and Yan, R. (2021) BACE1 controls synaptic function through modulating release of synaptic vesicles. *Mol. Psychiatry*, **26**, 6394–6410.

51. Treiber, H., Hagemeyer, N., Ehrenreich, H. and Simons, M. (2012) BACE1 in central nervous system myelination revisited. *Mol. Psychiatry*, **17**, 237–239.

52. Trimarco, A., Forese, M.G., Alfieri, V., Lucente, A., Brambilla, P., Dina, G., Pieragostino, D., Sacchetta, P., Urade, Y., Boizet-Bonhoure, B. *et al.* (2014) Prostaglandin D2 synthase/GPR44: a signaling axis in PNS myelination. *Nat. Neurosci.*, **17**, 1682–1692.

53. Li, L., Li, R., Zacharek, A., Wang, F., Landschoot-Ward, J., Chopp, M., Chen, J. and Cui, X. (2020) ABCA1/ApoE/HDL signaling pathway facilitates myelination and oligodendrogenesis after stroke. *Int. J. Mol. Sci.*, **21**, E4369.

54. Vnencak, M., Schölvinck, M.L., Schwarzacher, S.W., Deller, T., Willem, M. and Jedlicka, P. (2019) Lack of β-amyloid cleaving enzyme-1 (BACE1) impairs long-term synaptic plasticity but enhances granule cell excitability and oscillatory activity in the dentate gyrus in vivo. *Brain Struct. Funct.*, **224**, 1279–1290.

55. Ou-Yang, M.-H., Kurz, J.E., Nomura, T., Popovic, J., Rajapaksha, T.W., Dong, H., Contractor, A., Chetkovich, D.M., Tourtellotte, W.G. and Vassar, R. (2018) Axonal organization defects in the

hippocampus of adult conditional BACE1 knockout mice. *Sci. Transl. Med.*, **10**, eaao5620.

56. Lombardo, S., Chiacchiaretta, M., Tarr, A., Kim, W., Cao, T., Sigal, G., Rosahl, T.W., Xia, W., Haydon, P.G., Kennedy, M.E. *et al.* (2019) BACE1 partial deletion induces synaptic plasticity deficit in adult mice. *Sci. Rep.*, **9**, 19877.

57. Kim, H.-J., DiBernardo, A.B., Sloane, J.A., Rasband, M.N., Solomon, D., Kosaras, B., Kwak, S.P. and Vartanian, T.K. (2006) WAVE1 is required for oligodendrocyte morphogenesis and normal CNS myelination. *J. Neurosci.*, **26**, 5849–5859.

58. Zuchero, J.B., Fu, M.-M., Sloan, S.A., Ibrahim, A., Olson, A., Zaremba, A., Dugas, J.C., Wienbar, S., Caprariello, A.V., Kantor, C. *et al.* (2015) CNS myelin wrapping is driven by actin disassembly. *Dev. Cell*, **34**, 152–167.

59. Kasuga, Y., Fudge, A.D., Zhang, Y. and Li, H. (2019) Characterization of a long noncoding RNA Pcdh17it as a novel marker for immature premyelinating oligodendrocytes. *Glia*, **67**, 2166–2177.

60. Brewer, K.D., Shi, S.M. and Wyss-Coray, T. (2022) Unraveling protein dynamics to understand the brain - the next molecular frontier. *Mol. Neurodegener.*, **17**, 45.

61. Tsien, J.Z., Chen, D.F., Gerber, D., Tom, C., Mercer, E.H., Anderson, D.J., Mayford, M., Kandel, E.R. and Tonegawa, S. (1996) Subregion- and cell type-restricted gene knockout in mouse brain. *Cell*, **87**, 1317–1326.

62. Campsall, K.D., Mazerolle, C.J., De Repentingy, Y., Kothary, R. and Wallace, V.A. (2002) Characterization of transgene expression and Cre recombinase activity in a panel of Thy-1 promoter-Cre transgenic mice. *Dev. Dyn.*, **224**, 135–143.

63. McDade, E., Voytyuk, I., Aisen, P., Bateman, R.J., Carrillo, M.C., De Strooper, B., Haass, C., Reiman, E.M., Sperling, R., Tariot, P.N. *et al.* (2021) The case for low-level BACE1 inhibition for the prevention of Alzheimer disease. *Nat. Rev. Neurol.*, **17**, 703–714.

64. Dobin, A., Davis, C.A., Schlesinger, F., Drenkow, J., Zaleski, C., Jha, S., Batut, P., Chaisson, M. and Gingeras, T.R. (2013) STAR: ultrafast universal RNA-seq aligner. *Bioinformatics*, **29**, 15–21.

65. Satija, R., Farrell, J.A., Gennert, D., Schier, A.F. and Regev, A. (2015) Spatial reconstruction of single-cell gene expression data. *Nat. Biotechnol.*, **33**, 495–502.

66. Zheng, G.X.Y., Terry, J.M., Belgrader, P., Ryvkin, P., Bent, Z.W., Wilson, R., Ziraldo, S.B., Wheeler, T.D., McDermott, G.P., Zhu, J. *et al.* (2017) Massively parallel digital transcriptional profiling of single cells. *Nat. Commun.*, **8**, 14049.

67. Traag, V.A., Waltman, L. and van Eck, N.J. (2019) From Louvain to Leiden: guaranteeing well-connected communities. *Sci. Rep.*, **9**, 5233.

68. Polański, K., Young, M.D., Miao, Z., Meyer, K.B., Teichmann, S.A. and Park, J.-E. (2020) BBKNN: fast batch alignment of single cell transcriptomes. *Bioinformatics*, **36**, 964–965.

69. Hao, Y., Hao, S., Andersen-Nissen, E., Mauck, W.M., Zheng, S., Butler, A., Lee, M.J., Wilk, A.J., Darby, C., Zager, M. *et al.* (2021) Integrated analysis of multimodal single-cell data. *Cell*, **184**, 3573–3587.e29.